Chemical Engineering Science 131 (2015) 138–145

Contents lists available at ScienceDirect

Chemical Engineering Science

journal homepage: www.elsevier.com/locate/ces

Characterization of pore coking in catalyst for thermal down-hole upgrading of heavy oil

Paul Dim [a], Abarasi Hart [b], Joseph Wood [b], Bill Macnaughtan [c], Sean P. Rigby [a,*]

[a] Department of Chemical and Environmental Engineering, University of Nottingham, University Park, Nottingham NG7 2RD, UK
[b] Centre for Formulation Engineering, Department of Chemical Engineering, School of Engineering, The University of Birmingham, Edgbaston, Birmingham B15 2TT, UK
[c] Food Sciences, Sutton Bonington Campus, University of Nottingham, Sutton Bonington, Leicestershire LE12 5RD, UK

HIGHLIGHTS

- Novel experimental technique for studying coking.
- Method to understand spatial juxtaposition of coking pores.
- Assess impact of different process conditions on pore structure.
- Aid to design of deactivation-resistant catalysts.

GRAPHICAL ABSTRACT

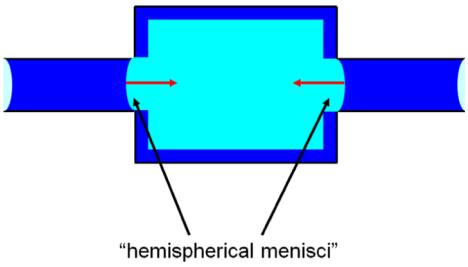

ARTICLE INFO

Article history:
Received 22 October 2014
Received in revised form
3 February 2015
Accepted 29 March 2015
Available online 3 April 2015

Keywords:
Bitumen
in-situ combustion
Thermoporometry
Adsorption
Porosity

ABSTRACT

Heavy oil and bitumen are a potential alternative energy source to conventional light crude. However, recovery of these resources can have substantial environmental impact. Downhole upgrading offers the prospect of both improving recovery, and decreasing environmental impact. However, use of catalysts to enhance downhole upgrading is limited by the need for one that can survive the extreme coking conditions arising from the cracking of heavy oil. In this work the potential of hydrogen donors to improve upgrading and enhance catalyst lifetime was considered. In order to extract detailed information on the catalyst structural evolution during reaction a novel parallel adsorption and thermoporometry characterization method was used. This technique allows detailed information to be obtained on the spatial juxtaposition of different pores, and their relative connectivity, as well as on size distributions. For catalyst operated at the conditions studied, it has been found that coking arises in smaller pores branching off the larger pores providing access to the catalyst interior. It has been found that while coking following use of different types of hydrogen donor leads to similar primary patterns of evolution in the pore-scale descriptors of the remaining accessible void-space, differences do arise in the overall accessible volume. Hence, it seems the hydrogen donor affects the location rather than general nature of the pore structure changes. However, at a secondary level of scrutiny, some differences in pore-scale evolution are also identified for different hydrogen donors. These differences identified helped the understanding of variations in the performance of different hydrogen donor and catalyst combinations.
© 2015 Published by Elsevier Ltd.

1. Introduction

Peak production of conventional light oil is likely to occur before 2035 (IEA, 2011). Thereafter there will be a decline in supply if alternative sources are not found and exploited. Heavy oil

* Corresponding author. Fax: +44 115 951 3898.
E-mail address: enzspr@exmail.nottingham.ac.uk (S.P. Rigby).

http://dx.doi.org/10.1016/j.ces.2015.03.052
0009-2509/© 2015 Published by Elsevier Ltd.

and bitumen represent a potential alternative to conventional oil. However, heavy oil and bitumen cannot be refined by conventional refineries without upgrading to convert them to synthetic light crude oil (Hart et al., 2013, 2014). Heavy oil and bitumen can be recovered using in-situ combustion. In-situ combustion methods involve burning part of the oil to recover the rest, by using the heat produced from the combustion reactions to reduce the viscosity of the remaining oil and allow it to flow to a producer well. One such method is the Toe-to-Heel Air Injection (THAI) method (Shah et al., 2010). In THAI, air is injected through a vertical injector well to supply the oxidant for a flame front which sweeps through the reservoir. The oil mobilized by the heat from the flame front flows down to a horizontal producer well towards the base of the reservoir. Very high temperatures, up to 600–700 °C can be obtained in the reservoir. Hence, the oil may undergo pyrolysis, and, also, upgrading reactions due to the natural catalytic activity of the host rock. The CAtalytic upgrading PRocess In-situ (CAPRI) is a way to further enhance the upgrading arising from the THAI process itself. In CAPRI the horizontal producer well is wrapped around with an annular packed-bed of upgrading catalyst. As the mobilized heavy oil flows towards the producer well it passes through the packed bed of catalyst and undergoes further upgrading reactions. While the catalyst lifetime need only be of the order of a few days, which is the time for the flame front region to pass a particular location, the conditions the catalyst experiences are severe.

The reactions involving heavy oil taking place on the catalyst are highly likely to produce solid carbonaceous deposits, generally called 'coke'. This coke can smother active sites, and/or prevent access of reactants to the catalyst pellets completely by blocking of surface pores. The spatial distribution of coke depends upon the balance between the rates of reaction and mass transfer. A rapid coking reaction, relative to the rate of mass transport, is likely to lead to pore-mouth blocking, whereas a slower reaction is likely to lead to a more even distribution of coke. The rate of mass transfer is affected by the pore structure of the catalyst pellet.

Hart et al. (2013), successfully demonstrated that with better control of the oil flow, injected hydrogen can significantly improve the quality of the produced oil and reduce the coke build up on the surface of the catalysts. However due to the difficulties and expense of supplying gaseous hydrogen to the well, hydrogen donor solvents may be considered as an alternative. Cyclohexane and tetralin are widely used as hydrogen donor solvents for industrial applications such as nylon and coal liquefaction respectively. Dehydrogenation of cyclohexane for hydrogen storage and supply, as well as the use of tetralin as a donor solvent for coal/oil shale liquefaction and thermal/catalytic upgrading of heavy vacuum residues, have been extensively documented (Biniwale et al., 2005; Peden and Goodman, 1987; Liu and Fan, 2002; Alemán-Vázquez et al., 2012). In this study both of these solvents have been used as a potential source of continuous supply of hydrogen for the CAPRI catalyst to effect upgrading and as diluent for higher recovery.

The pore structures of catalysts are generally characterized using techniques such as gas adsorption. An additional technique, which is gaining popularity, is thermoporometry. However, these techniques have problems with pore-pore interaction phenomena affecting the accuracy of the pore size distributions for disordered solids that are particularly acute for coked catalysts (Gopinathan et al., 2013). However, these issues, which will be described in more detail below, can be overcome by the novel integrated method used in this paper (Shiko et al., 2012). In this work, rather than using gas sorption or thermoporometry separately, we will combine them into a composite technique. This new technique consists of performing thermoporometry studies using the adsorbate from an adsorption experiment as the probe fluid at different levels of pellet saturation (with adsorbate). As will be seen below, this novel method delivers much more information on the relative proximity and connectivity of pores affected by coking or left open, and thereby gives a more detailed picture of the coking process. This more detailed picture of pore structure evolution during coking enables a better idea of how to make catalysts more resistant to coking to be obtained.

In this work, we will look at the potential benefits of using a guard bed of activated carbon to protect the catalyst from deactivation, and the impact of the use of various different hydrogen sources for improving upgrading on coking. In particular, the aim of this work is to study the effects of the combination of choice of hydrogen source and a particular catalyst pore structure has on coking resistance for that catalyst. This is to enable a more informed selection of hydrogen source for a given catalyst.

2. Theory

2.1. Gas sorption

Pore structural characterization by gas sorption is based on the phenomenon of capillary condensation. The Kelvin equation (Rouquerol et al., 1999) suggests that the logarithm of the relative pressure at which a vapour will condense within a pore is inversely proportional to the pore size:

$$\ln\left(\frac{P}{P_0}\right) = -\frac{k\gamma V_m \cos\theta}{RT(r_p)} \quad (1)$$

where P/P_o is the relative pressure at which condensation occurs in a cylindrical pore of radius r_p, k is a geometry parameter and depends on the pore and meniscus geometry (for a cylindrical pore open at both ends $k=1$; and for a pore with one dead end, or for adsorption from a hemi-spherical meniscus, $k=2$), γ is the surface tension and V_m is the molar volume of the condensed liquid phase, θ is the contact angle with which the liquid meets the wall, and T is the absolute temperature. Based on the Kelvin equation, the relative pressure needed to condense vapour in a through cylindrical pore, with a sleeve-shaped meniscus formed by the surface adsorbed layer, is the square root of the relative pressure needed to condense vapour starting from a hemispherical meniscus formed at the end of a dead-end cylindrical pore (Rouquerol et al., 1999). This sensitivity to meniscus geometry means there is not necessarily a monotonic relationship between the applied pressure and the characteristic size of pore in which condensation will have occurred for inter-connected, disordered solids.

In a through ink-bottle pore geometry, consisting of a large pore body sandwiched between two narrower necks, the presence of the larger body may be concealed by the 'advanced condensation effect', originally proposed by De Boer (1958). As illustrated in Fig. 1, condensation in the pore necks via a cylindrical sleeve-shaped meniscus will lead to the development of hemispherical menisci at the two entrances either end of the pore body. If the pressure for this neck-filling process exceeds that for filling of the pore body via a hemispherical meniscus, then the body will also fill simultaneously with the necks, and the two different pore sizes will appear as one. The physical occurrence of the advanced condensation effect has been observed experimentally using both integrated mercury porosimetry (Hitchcock et al., 2014) and magnetic resonance imaging methods (Hitchcock et al., 2010). The advanced adsorption effect, also known as the 'cascade effect', has also been seen in Monte-Carlo simulations of gas adsorption (Coasne et al., 2007).

The 'advanced condensation effect' (De Boer, 1958) is a particular problem when studying coking catalysts with gas sorption

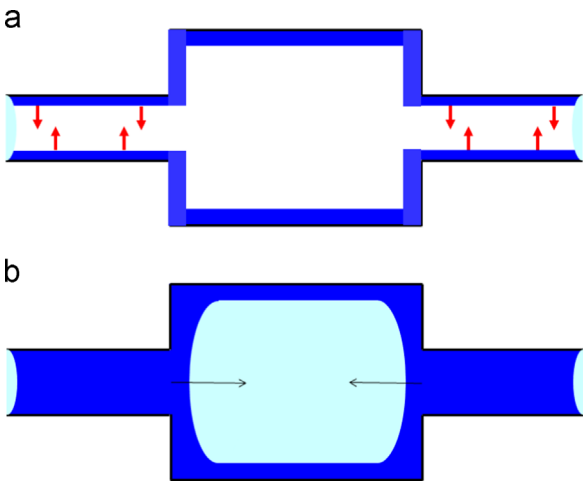

Fig. 1. Schematic diagrams showing the stages of the advanced condensation effect in a cylindrical through ink-bottle pore. (a) Condensation in pore necks via a cylindrical-sleeve type meniscus at pressure P_1, immediately followed by (b) filling of pore body via ingress of hemispherical menisci formed at ends.

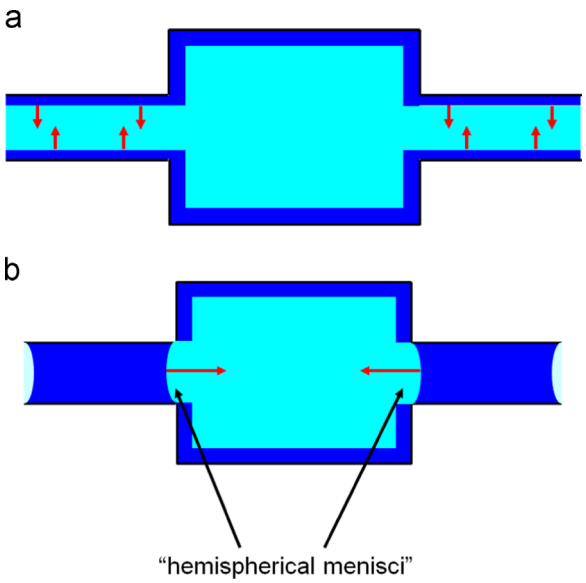

Fig. 2. Schematic depiction of the stages of the advanced melting process in a cylindrical, through ink-bottle pore system. The dark shading indicates the non-freezing surface liquid-like layer, while the light shading indicates the bulk frozen fluid. The arrows indicate the direction of the meniscus movement on initiation of melting from (a) sleeve-shaped menisci in the pore necks, and (b) hemispherical menisci at the entrances to the pore body.

because a situation of pore-mouth blocking with coke can give rise to the through ink-bottle geometry described above, but appear (from characterization data) to be more pervasive, complete site-coverage because the newly narrowed neck and remaining empty body fill with condensate as one. This is because the entire length of a coked pore may fill with condensate at a lower pressure than before even if just the pore mouth region has been narrowed by coke. It will then look like the size of the whole pore has been reduced by coke deposition, rather than just the entrance. Alternatively, if an ink-bottle geometry already exists, then coking of the pore mouth may make the neck size drop below the critical value required to permit advanced condensation, and create a spurious, apparent growth in the volume of pores with a large body size that might be mistaken for structural damage by the coke.

2.2. Thermoporometry

Thermoporometry makes use of the Gibbs–Thomson effect, whereby small crystals of a solidified probe fluid located within pores melt at a lower temperature than the bulk liquid (Riikonen et al., 2011). The melting point depression is inversely proportional to the crystal size, where the constant of proportionality depends upon the meniscus geometry between the solid and the melt. The melting process for the frozen phase is initiated from existing molten phase, such as the liquid-like layer that is always retained at the pore wall for ice crystals that do not wet the solid. This is shown in Fig. 2 for a through ink bottle pore model; the arrows show how the liquid-like layer initiates the melting process and this melting mechanism is said to occur via sleeve-shaped menisci. For such a melting mechanism, the smaller necks will melt first, and, then, as the temperature is raised, the large pore will also melt. Therefore, this type of melting event would give an accurate measurement of the both the neck and body sizes.

However, in cylindrical pores, melting could occur at a lower temperature via a hemispherical meniscus (between solid and molten phases), than it would via a sleeve-shaped meniscus. For the through ink bottle pore in Fig. 2, melting is initiated in the outer narrow necks from the thin cylindrical sleeve of permanently unfrozen liquid-like fluid that exists at the pore wall. Once the necks have become fully molten, a hemispherical meniscus will have consequently formed at both ends of the larger pore body. The hemispherical menisci could then initiate the melting process in the large pore provided the larger pore radius is smaller than the critical size for melting via a hemispherical meniscus at the current temperature. In that case the larger pore would melt at the same temperature as the smaller pore. Hence, what is in actuality two different pore sizes, would appear as just one from the melting curve. This is known as the advanced melting effect, and has been observed experimentally (Hitchcock et al., 2011).

While, as has been seen above, both gas sorption and thermoporometry are affected by pore-pore interaction phenomena, leading to a narrowing (relative to reality) of the measured pore size distribution, previous work (Shiko et al., 2013) has shown that the critical ratio of the sizes of neighboring pores to permit these effects to occur is different. Hence, an integrated combination of the two techniques can be used to detect these effects in each other, and, thereby, infer information on the proximity of pores of given sizes. The data-set for the fully-integrated method is much richer in implicit information on the connectivity of different pores than the data for the individual techniques alone taken together. This synergistic effect will be used to study the spatial distribution of coke lay-down in the upgrading catalysts.

2.3. Mass transport

When diffusion within a porous solid is accompanied by adsorption, a simple mass balance shows that the usual diffusion equation (here for a sphere with radial co-ordinate r) must be modified (Crank, 1975) to allow for this:

$$\frac{\partial C}{\partial t} = \frac{D_e}{(H+1)}\left[\frac{\partial^2 C}{\partial r^2} + \frac{2}{r}\frac{\partial C}{\partial r}\right], \tag{2}$$

where D_e is the (purely mass transport) effective diffusivity, and H is the constant of proportionality between the concentrations of the adsorbed phase and the freely diffusing phase (in the appropriate units). If there is a linear relationship between the concentrations of the surface adsorbed phase and the freely diffusing phase then solutions of the diffusion with adsorption problem, for given initial and boundary conditions, are the same as for the corresponding problem in simple diffusion except that the modified diffusion coefficient $D_e/(H+1)$ is used. Beyond the Henry's law region, the assumption of a linear relationship between the

concentrations of the adsorbate in the gas phase and adsorbed phase usually only applies over a limited pressure range. Ideally, a plot of concentration of adsorbed phase against concentration in the gas phase would be acquired using very tiny pressure steps over which the assumption of linearity would be most accurate, but, in order to improve the signal-to-noise ratio in the data, larger pressure steps are actually used. In this work H was derived from the tangent to the adsorption isotherm at the upper isotherm point for the mass-uptake step.

A simple, and often-applied, intra-particle mass-transfer model is the so-called Linear Driving Force (LDF) model, where uptake data fitted to the expression:

$$\frac{M(t)}{M(\infty)} = 1 - \exp(-kt). \quad (3)$$

where k is a mass transfer coefficient (MTC), which is proportional to D_e/a^2, where a is a characteristic diffusion path length. In the real constant pressure experiment it is impossible to obtain a perfect step-function increase in external pressure, and thus the boundary condition is an approximation. The approximation is generally reasonable as the time taken for the pressure increase is small in comparison with the time required to reach adsorption equilibrium. For diffusion within porous solids, the area for diffusion is reduced to the voidage fraction. The diffusivity is further reduced by the factor of the tortuosity, representing deviations from straight-line paths for the diffusive flux. The temperature dependence for bulk diffusion in gases is $\sim T^{3/2}$.

3. Method

CAPRI, the catalytic extension of the THAI process, was investigated using a fixed bed microreactor and laboratory scale experimental rig for heavy crude oil upgrading in the presence of hydrogen donors, such as hydrogen gas, or solvents like cyclohexane and tetralin at two different ratios of THAI oil/Hydrogen donor solvent of 9:1 and 5:1. To simulate the downhole CAPRI process, partially upgraded (THAI feed 3, dentoted T3; 14° API and viscosity 1.091 Pa s) Kerrobert, Canada, heavy crude oil was used as feed under previously optimised operating temperature of 425 °C and 20 barg pressure in a nitrogen atmosphere using HDS/HDT CoMo/Alumina catalyst. The gas flow-rate was 500 ml min^{-1}, and the gas-to-oil volumetric ratio was 500:1. The reaction time in the reactor before discharge of the coked samples was 8 h. The spent catalyst samples for which the pore structure was characterized using the integrated adsorption-thermoporometry method include the fresh and four coked CoMo/γ-Al_2O_3 samples, as shown in Table 1.

The methods for the characterization studies of the fresh and coked catalyst samples were as follows. The samples were saturated with water using a Series 3 Climate chamber TAS apparatus at 25 °C and a Relative Humidity (RH) in the range 75-100%. To obtain saturated accessible pore volume values for water, samples were left for 11 days to reach equilibrium, when no further significant mass increase occurred. Comparison of the adsorbate volumes for water, at 100% RH, and nitrogen adsorption at 77 K (Hart et al., 2013, 2014) suggest that water fully wets the coked samples by vapour sorption.

For thermoporometry experiments, about 15–30 mg of the partially-, or fully-, saturated samples were sealed into a pre-weighed DSC aluminium hermetic pan (TA Instruments, Part #900793.901 for bottom and Part #900794.901 for lid). The partially saturated samples had been equilibrated at one of 75%, 85% or 95% RH. The DSC pans were weighed after addition and sealing of the saturated samples. The pan was subsequently introduced into the furnace of the DSC. A differential scanning calorimeter (Q10 DSC, TA Instruments) equipped with a cooling unit (RCS, Refrigerated Cooling System) for controlled cooling and sub-ambient temperature operation was used. A constant furnace atmosphere was maintained with an in-house nitrogen purge.

The DSC thermoporometry measurements were performed as follows. The sample was cooled to −50 °C and that temperature was maintained for 30 min to ensure that all of the water was frozen. After that, the sample was heated to 5 °C at a heating rate of 0.5 °C/min and the temperature was maintained for 10 min. After completing the DSC measurements, the sample pans were reweighed to check that no water had escaped during the experiment. The DSC measurements were repeated on three samples of the same material, with the same conditions. It is important to use the same heating rate throughout the experimental run; otherwise the results are influenced by the heating rate. This procedure was also repeated using two further heating rates of 1.0 and 1.5 °C/min, respectively, to check whether findings were independent of heating rate. No significant effect of heating rate was observed, and thus the data reported is for 1.5 °C/min. The data were analyzed assuming a Gibbs–Thomson parameter of 50 K nm^{-1} (based on diameter), typical for oxide materials (Schreiber et al., 2001).

A dynamic vapour sorption analyzer (DVS-1 Surface Measurement Systems Ltd. London UK) equipped with a Cahn D200 microbalance was used to measure the water sorption isotherms of the catalyst samples. Relative Humidity (RH) calibration of the system was by means of the deliquescent point of saturated salt solutions. Experiments were carried out at a temperature of 293 K, or of 297 K, and stepped RH values ranging from 0% to 95%. The initial weight of the samples was in the region of 10 mg. Catalyst samples were used in the form of 2–3 intact pieces and initially weighed on a normal laboratory balance external to the DVS before being placed in quartz hemispherical holders in the DVS. Samples were initially pre-dried in the DVS by passing dry air over the pieces until equilibration. The dry samples were subsequently hydrated using several different RH programs involving adsorption and desorption. Samples were considered equilibrated when the change in mass per unit time was less than 0.0005 mg/min, or the equilibration time had reached the maximum step value; in some cases 720 min. The isotherm data presented here was equilibrated. Using this procedure, the moisture content expressed as a percentage on a dry weight basis could be plotted against RH and the isotherm obtained.

The coke content of the catalyst after upgrading was determined using a thermogravimetric analyser (TGA) NETZSCH-Geratebau GmbH, TG 209 F1 Iris®. The analysis was carried out

Table 1
Coked catalyst samples studied in this work.

Sample code	Sample description
A	CoMo/alumina + H_2 in feed
B	CoMo/alumina + activated carbon guard bed + THAI 3 experimental oil and cyclohexane (9:1 ratio)
C	CoMo/alumina + activated carbon guard bed + THAI 3 experimental oil
D	CoMo/alumina + activated carbon guard bed + THAI 3 experimental oil and tetralin (9:1 ratio)

using a ramp temperature increase from 25 to 900 °C under air flow of 50 mL min^{-1}. A detailed description of the method has been reported in Hart et al. (2013, 2014).

4. Results and discussion

The results from the reactor studies are summarized in Table 2. Note the feed oil API gravity and viscosity are 14° API and 1.091 Pa s. From Table 2, it is clear that the produced oil API gravity after upgrading under hydrogen atmosphere gave the highest increment compared to hydrogen-donor solvent. This is because during the upgrading the cleavage of a macromolecule and the addition of hydrogen from dehydrogenation of tetralin and cyclohexane to form a stable molecule leads to the formation of naphthalene and benzene. The polymerized form of these aromatic molecules produced as a result of the release of hydrogen from the solvent induces high density (inverse of API gravity) to the upgraded oil. However, the dissociation of hydrogen produces the lightest radicals to help suppress macro-radicals polymerization and promote hydrogenation reactions to stable and smaller molecules. Correspondingly, the level of viscosity reduction is approximately the same within an error margin. The level of improvement in API gravity and viscosity after upgrading is an indication of coke deposition on the catalyst. The catalyst coke content after upgrading was determined by thermogravimetric analyser. The high coke content after upgrading with tetralin and cyclohexane compared to hydrogen could be attributed to the formation of aromatics due to dehydrogenation to release hydrogen. These aromatics are known coke precursors during reaction.

The nitrogen adsorption isotherms for fresh and representative coked catalysts have been reported in the supplementary materials. Fig. 3 shows the water adsorption isotherms for some examples of the coked catalysts, and also the fresh catalyst. The isotherms were obtained at 297 K except for sample C which was obtained at a slightly lower temperature of 293 K to increase uptake and thus improve signal-to-noise. It can be seen that the water adsorption isotherms for the fresh catalyst and coked catalyst C are Type II in form according to the IUPAC classification scheme (Rouquerol et al., 1999), while that for coked catalyst A is Type III. A Type III shaped isotherm is associated with weaker adsorbate–adsorbent interaction strength than Type II. This finding suggests that either the coke chemistry for sample A is more hydrophobic than that for sample C, and/or the coverage of still accessible surface, by a coke more hydrophobic in nature than fresh catalyst surface, is more pervasive for sample C. The isotherms for samples B and D were Type III.

Table 2
Coke content of deactivated catalyst pellets and oil upgrading parameters obtained from reaction studies.

Reactants	Coke content (wt %)	Average API #gravity rise (deg)	Viscosity reduction (%)
CoMo+AC+feed oil/cyclo (9:1)+N_2	28.21	2.8 ± 0.7	87.0
CoMo+AC+feed oil/cyclo (5:1)+N_2	26.55	2.6 ± 0.7	86.0
CoMo+AC+feed oil/tetr (9:1)+N_2	26.31	3.0 ± 0.8	89.0
CoMo+AC+feed oil/tetr (5:1)+N_2	27.74	2.9 ± 0.7	86.7
CoMo+AC+feed oil+H_2	26.58	3.3 ± 0.9	86.5

Notes: cyclo=cyclohexane, tetr=tetralin and THAI 3=feed oil, AC=activated carbon guard bed and CoMo/Al_2O_3.

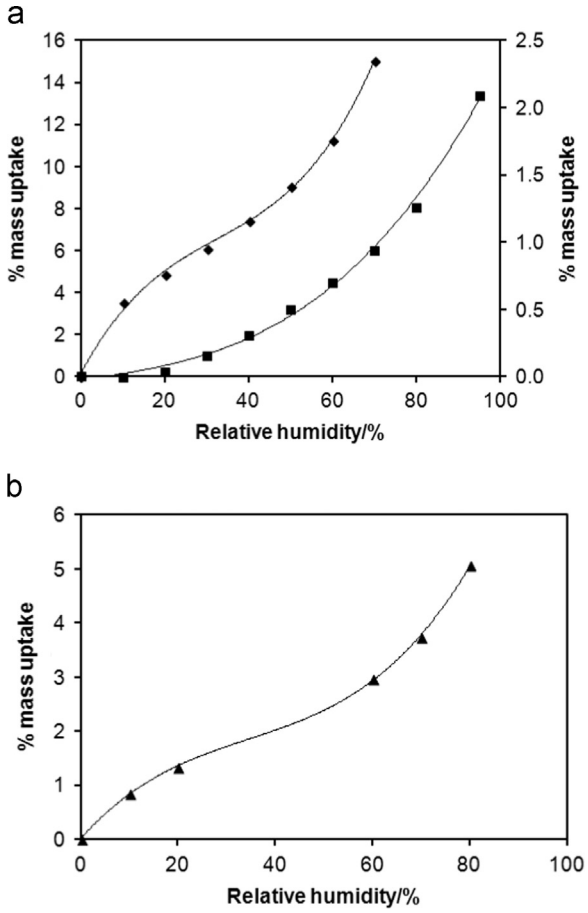

Fig. 3. Water adsorption isotherms for (a) fresh catalyst at 297 K (♦, left-hand axis), sample A at 297 K (■, right-hand axis); and (b) sample C at 293 K. The lines shown are to guide the eye.

Table 3
Water adsorption mass transfer coefficients, corrected for adsorption, for fresh and coked catalysts. The coefficients are all those measured/calculated for a temperature of 297 K.

Sample code	Accessible void volume to water/(ml g^{-1})	Mass transfer coefficient/min^{-1}
Fresh catalyst	0.47	1440
A	0.28	17.0
B	0.11	37.4
C	0.22	115
D	0.05	119

Table 3 shows the accessible void volume for water (determined from water saturation at 100% RH), and the water mass transfer coefficients (MTCs), corrected for adsorption, obtained for the fresh and coked catalysts at low (sub-monolayer) surface coverage during the water adsorption experiment. It can be seen that the MTCs increase in the order A to D, and all are at least an order of magnitude less than for the fresh sample. There is no correlation between accessible void volume and size of MTC. Even though sample A had a Type III water adsorption isotherm, it still has a relatively high overall pore volume accessible to water. This suggests that water-wetting effects (e.g. exclusion from open but completely hydrophobic pores) are not important at high saturation levels in coked catalysts.

Fig. 4 shows the DSC curves for the water in fresh catalyst equilibrated at different relative humidities. At 75% RH the size distribution is very broad, with the modal peak at ~2.5 nm and a

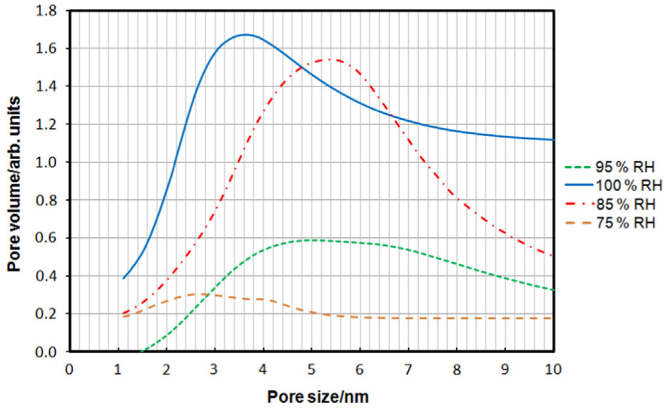

Fig. 4. DSC thermoporometry melting curve pore size distributions (histograms) for fresh CoMo catalyst for water saturation equilibrated at four different relative humidities. Pore volumes for each sample are not on the same absolute scale.

pronounced shoulder at ~4 nm. As the RH is increased to 85% and more water is adsorbed, then the DSC modal peak shifts to a larger size of ~5 nm, but remains relatively narrow. As the RH is increased further to 95%, the modal peak becomes substantially broadened towards larger pore sizes. In the final dataset where the RH has been increased to 100%, the modal peak of the DSC curve shifted back to lower size of ~3.5 nm. The shift in the modal peak position suggests that, as RH is increased from 75% to 95% steadily larger pore sizes are filled with water. Once the final empty pores are filled by increasing the RH to 100%, the change in the direction of the movement of the modal peak shift with increased RH signified the onset of substantial percolation of the melting front due to the pervasiveness of advanced melting. Pores of size ~3.5 nm (based upon a Gibbs–Thomson parameter of 50 K nm^{-1}) are facilitating the advanced melting of a large fraction of larger pores, and thus must be in immediate proximity to these pores. When the potential for significant advanced melting exists (as the highest RH results suggest occurs for the CoMo/alumina catalyst studied here), when the melting curve peak broadens, as it does at intermediate RH values, this suggests the water is adsorbing at these RH values is doing so in relatively segregated regions of the pellet, as no advanced melting occurs to obscure the presence of larger pores. Hence, the results from the hybrid adsorption-thermoporometry method implicitly contain information on the spatial juxtaposition of pores of different sizes.

Fig. 5 shows the DSC curves for fully saturated samples of fresh catalyst and the various catalysts discharged following upgrading reactions under different conditions. It can be seen that the general finding is that the modal peak of all of the used catalyst samples has shifted to ~5–6 nm, away from ~3.5 nm for the fresh catalyst. However the width of the DSC curve peak declines in the order C to D to B to A. Since, generally, coking can be expected to lead to larger pores being made smaller or rendered inaccessible (Mann et al., 1996), the shift in the modal peak to larger size suggests, rather, that the coking has reduced the incidence of advanced melting present in the fresh catalyst. This could occur if the smaller pores facilitating melting for the larger pores were either blocked entirely, or reduced in size such that they fall below the critical size to permit advanced melting. The differences in the apparent width of the size distributions for different spent catalysts suggest that more smaller pores are preserved under some reaction conditions than others. A larger volume of smaller pores are increasingly preserved in the order A, B, D, to C. It is noted that the level of preservation of the smaller pores for coked samples in Fig. 5 correlates well with increasing MTC in Table 3. However, the similarity in the position of the modal peak for all spent catalysts suggests that the particular small pores (that

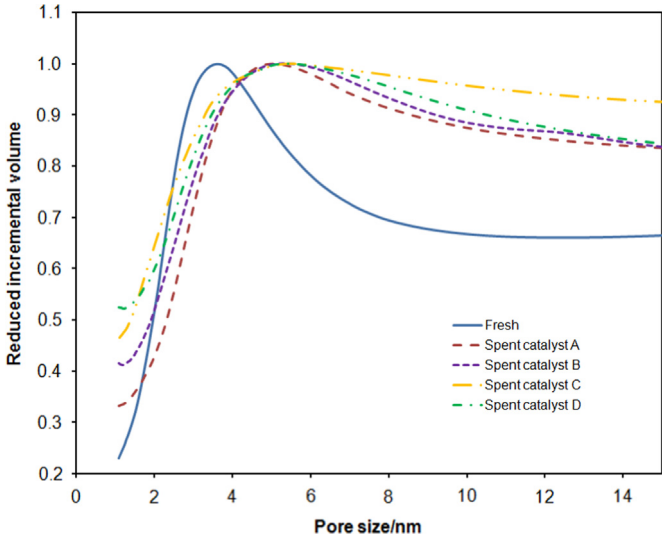

Fig. 5. Pore size distribution obtained from DSC thermoporometry melting curve for fully saturated fresh and spent CoMo catalyst samples. The curve represents a histogram of incremental volume (reduced by maximum incremental volume) against pore size.

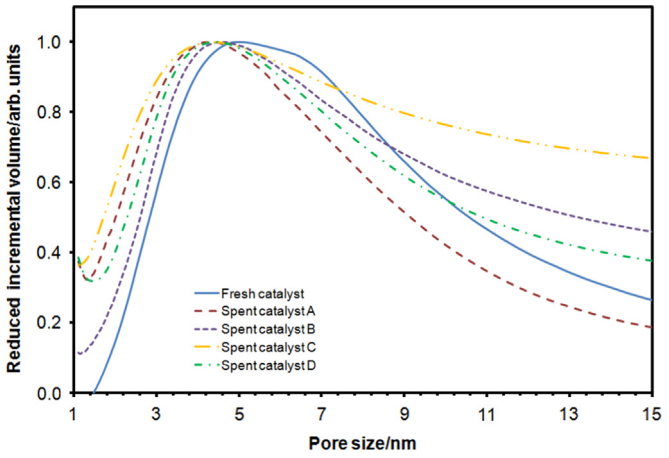

Fig. 6. Pore size distribution obtained from DSC thermoporometry melting curve for partially saturated fresh and spent CoMo catalyst samples equilibrated at 95% RH. The curve represents a histogram of incremental volume (reduced by maximum incremental volume) against pore size.

facilitate advanced melting at low temperature) in close proximity to the larger pores are rendered inaccessible in all conditions.

Fig. 6 shows the DSC curves for fresh and spent catalyst samples after partial saturation with water by equilibration at 95% RH. It can be seen that the position of the modal peak is similar for all samples, including the fresh catalyst. This contrasts with the corresponding data obtained at 100% RH, where the modal peak for the spent catalyst samples was significantly displaced relative to that of the fresh catalyst. The position of the modal peak for the spent catalysts has declined very slightly from around 5–6 nm to around 4–5 nm. The modal peak for the fresh catalyst is at about 5 nm, and is the narrowest of the samples studied. The similarity of the position of the modal peak for fresh catalyst equilibrated with water vapour at 95% RH to the position of the modal peaks for spent catalysts at both 95% and 100% RH suggests that those pores rendered inaccessible by coking are likely to be the same pores in the fresh sample that facilitated advanced melting of the pores that fill with condensed water at the highest vapour pressures corresponding to RH between 95% and 100%.

In addition to the aforementioned primary effect of coking on pore-scale properties, implicit in the position of the modal DSC peak, consideration of the width of the DSC curve reveals secondary level changes to the pore structure on coking. It is noted that, the DSC curve for coked sample D saturated to 95% RH is broader than for the fresh catalyst, as was the corresponding curve for the fully saturated sample. However, in contrast, the DSC curve for sample A in Fig. 6 is, instead, shifted as a whole towards smaller pores, relative to the fresh catalyst data. The wider curve for sample D may indicate that the large and small pore sizes in the curve are well segregated by either connections blocked by coke or that no longer fill with condensate because of coking. This finding suggests some differences in the pattern of coke lay-down between the sets of conditions giving rise to coked samples A and D.

From a comparison of the data in Figs. 5 and 6 it can be seen that the modal peak for the DSC curves for coked catalysts shifts from ~4 nm, to a slightly larger pore size of ~5 nm, on increasing RH from 95% to 100%. If a higher relative pressure were required to condense water in smaller, but hydrophobic, coked pores, compared to remaining larger fresh pores, then it would be expected that this increase in modal pore size in the DSC data would not occur. Further, if a coked surface was relatively non-wetting for water, compared with the fresh catalyst surface, then the Gibbs–Thomson equation predicts, ignoring any advanced melting effects, that the melting point depression would be larger in magnitude for water imbibed in a coked pore. Hence, the modal peak for coked samples in Fig. 5 might be expected to have shifted to smaller pore sizes, compared to the fresh sample. However, this is not what was observed in Fig. 5. Although there is a shift to lower pore sizes for the modal melting peak for partially-saturated coked samples in Fig. 6, since a similar effect was not seen in Fig. 5, then this suggests that the effect in Fig. 6 must be due to structural change from coke deposits, not due to changes in wetting properties of the surface.

The most pronounced pattern in the findings given above, namely the shifts in the relative positions of the modal peaks, can be understood in terms of a simple corrugated pore model, as shown in Fig. 7(a). The thermodynamic aspect of the model assumes that the critical pore size ratio for permitting advanced phenomena is smaller for gas adsorption than for melting in thermoporometry, such that advanced melting occurs for some pores when advanced adsorption does not. The structural aspect of the model consists of a series of cylindrical pore elements of different diameters arrayed in series. The entrance to the pore from outside the pellet enters a medium sized pore segment, followed by large and small segments in that order when penetrating deeper into the solid. During adsorption of water vapour, if the ratio of sizes of neighboring pores exceeds the critical value for advanced adsorption, then the three different pores will fill independently in order of increasing size from 1 to 3. However, if the ratios of the sizes of the large and medium pores to that of the small one does not exceed the critical ratio for advanced melting of the condensate, then the modal melting peak will first shift from low to higher temperature as the, initially segregated, small and medium segments fill up, but then shift back to low temperature when the intermediate large pore fills, since then a pervasive pathway would allow the melting front to advance from the small pore throughout the pore system at a lower temperature. If (as in Fig. 7(b)) the interior small pore segment is completely blocked by coking in the spent catalyst, then the medium and large pore segments would still remain accessible to the outside and the condensing vapour. Hence, the modal melting peak for a fully water-saturated pore space will correspond to the size of the medium-sized pore segment, as melting would be then initiated at the medium pore segment, also leading to advanced melting of ice within the large segment. At the water saturation level equilibrated with 95% RH, the large pore segment would not be filled, and the melting modal peak will be dominated by the medium pore segment size for fresh and coked catalysts, as advanced melting cannot arise in either case.

The MTCs for coked catalysts were much reduced compared to the fresh catalyst but varied significantly between different reaction conditions. It is noted, in Table 2, that the total coke content for all discharged catalysts was very similar for all reaction conditions. However, the differences in MTC and accessible pore volume suggest that it was the spatial disposition of the coke that changed with reaction conditions, rather than amount. Reductions in MTC are associated with a decrease in voidage fraction, and/or an increase in void space tortuosity, and/or an increase in diffusion path length. Coking is unlikely to lead to an increase in diffusion path length in the mechanically-stable pellets, but could reduce the voidage fraction, or increase the tortuosity, of the remaining accessible void volume. A concentration of impervious coke towards the centre of a pellet, or as an annular shell barrier at some distance from the centre, leading to a loss of accessible pore volume, would cause a decrease in diffusion path-length and an increase in MTC. The low MTC but high accessible pore volume for coked sample A is consistent with the spatial arrangement of coke being more dispersed (like currants in a currant-bun) such that

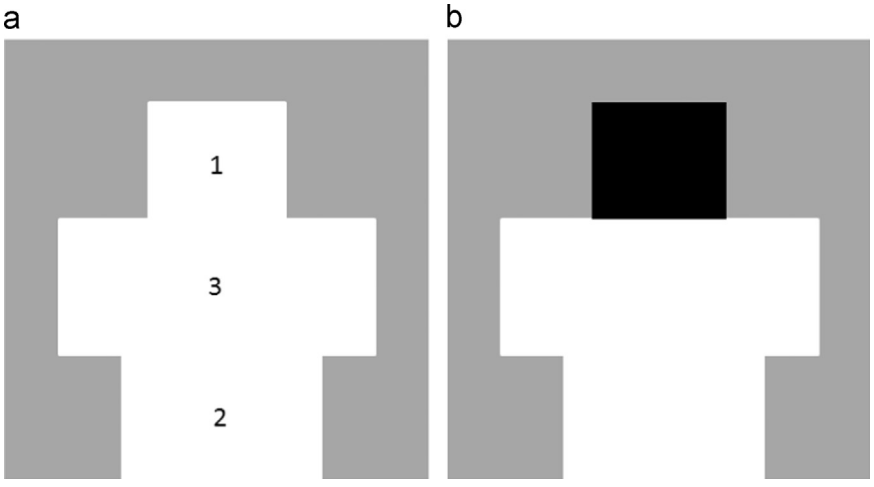

Fig. 7. Schematic diagram of pore model for fresh (a) and coked (b) catalyst, as described in the main text. The numerals in (a) denote the order in which the pores would fill with condensate.

water can still penetrate to the centre but through a tortuous path winding around pores blocked by coke deposits. In contrast, the relatively higher value of the MTC, and much lower accessible pore volume, for coked sample D is consistent with the coke substantially reducing the diffusion path length as well as increasing tortuosity overall. Sample B has both a low accessible pore volume and a low MTC suggesting that the coke occludes access to a lot of pores producing a highly tortuous path but that still penetrates relatively deep into the pellet compared to sample D. Sample C has both a relatively high accessible pore volume and a relatively high MTC compared to the other coked catalysts, suggesting that the spatial distribution of coke is highly probably heterogeneous but not completely blocking access to a central zone. The relatively low accessible pore volume for the spent catalysts discharged following addition of small hydrocarbon molecules as a hydrogen source suggests that the coking reaction occurs closer to the pellet surface than in conditions A and C. Hence, the coking reaction is more rapid. The gross similarity of the DSC data, for the different coked samples, to each other, combined with the difference in accessible volumes and MTCs, suggests that the mechanism of coking at pore-scale is similar but penetrates to different zones of the catalyst depending on reaction components.

5. Conclusions

In this work, the particular individual pathways for the structural evolution of the same catalyst, but coked under different reaction conditions, has been revealed by the pattern of similarities and differences amongst the results of various structural characterization methods for discharged coked samples. The combined adsorption and thermoporometry method has been used to probe the impact of coking on the overall pore size distribution and the pore-scale connectivity of pores of different sizes, while the water accessible pore volume and MTC have been used to probe the macro-scale spatial distribution of coke. It has been found that coking under otherwise similar reaction conditions, but with different hydrogen donors, affects the larger-scale spatial distribution of coke within a catalyst pellet, but not the overall amount deposited. Variations in accessible network tortuosity do not necessarily correlate with remaining penetrable depth into the pellet. Further, changes in the apparent modal size and connectivity of the remaining pore size distribution are generally independent of the depth of penetration of the coking front within the pellet. However, some differences are revealed in the more second-order features of the shape of the remaining pore-size distributions for coked catalysts obtained under different conditions. Overall, the same pore-scale coking mechanism seems repeated at different coking penetration depths for different hydrogen sources. It has also been shown how the advanced melting effect is critical to interpretation of thermoporometry data for porous catalysts.

Acknowledgements

The authors acknowledge the financial support of PTDF, Nigeria.

Appendix A. Supporting information

Supplementary data associated with this article can be found in the online version at http://dx.doi.org/10.1016/j.ces.2015.03.052.

References

Alemán-Vázquez, L.O., Cano-Domínguez, J.L., García-Gutiérrez, J.L., 2012. Effect of tetralin, decalin and naphthalene as hydrogen donors in the upgrading of heavy oils. Procedia Eng. 42, 532–539.
Biniwale, R.B., Kariya, N., Ichikawa, M, 2005. Dehydrogenation of cyclohexane over Ni based catalysts supported on activated carbon using spray-pulsed reactor and enhancement in activity by addition of a small amount of Pt. Catal. Lett. 105, 83–87.
Coasne, B., Galarneau, A., Di Renzo, F., Pellenq, R.M.J., 2007. Effect of morphological defects on gas adsorption in nanoporous silicas. J. Phys. Chem. C 111, 15759–15770.
Crank, J., 1975. The Mathematics of Diffusion. Clarendon Press, Oxford.
De Boer, J.H., 1958. The shapes of capillaries. In: Everett, D.H., Stone, F.S. (Eds.), The Structure and Properties of Porous Solids. Butterworths Scientific Publications, London, p. 68.
Gopinathan, N., Greaves, M., Wood, J., Rigby, S.P., 2013. Investigation of the problems with using gas adsorption to probe catalyst pore structure evolution during coking. J. Colloid Interface Sci. 393, 234–240.
Hart, A., Shah, A., Leeke, G., Greaves, M., Wood, J., 2013. Optimization of the CAPRI process for heavy oil upgrading: effect of hydrogen and guard bed. Ind. Eng. Chem. Res. 52, 15394–15406.
Hart, A., Leeke, G., Greaves, M., Wood, J., 2014. Downhole heavy crude upgrading by CAPRI: effect of hydrogen and methane gases upon upgrading and coke formation. Fuel 119, 226–235.
Hitchcock, I., Chudek, J.A., Holt, E.M., Lowe, J.P., Rigby, S.P., 2010. NMR studies of cooperative effects in adsorption. Langmuir 26, 18061–18070.
Hitchcock, I., Holt, E.M., Lowe, J.P., Rigby, S.P., 2011. Studies of freezing–melting hysteresis in cryoporometry scanning loop experiments using NMR diffusometry and relaxometry. Chem. Eng. Sci. 66, 582–592.
Hitchcock, I., Lunel, M., Bakalis, S., Fletcher, R.S., Holt, E.M., Rigby, S.P., 2014. Improving sensitivity and accuracy of pore structural characterisation using scanning curves in integrated gas sorption and mercury porosimetry experiments. J. Colloid Interface Sci. 417, 88–99.
International Energy Agency (IEA) (2011). World Energy Outlook. ISBN 978 9264 12413.
Liu, Y., Fan, H., 2002. The effect of hydrogen donor additive on the viscosity of heavy oil during steam stimulation. Energy Fuels 16, 842–846.
Mann, R., Khalaf, K., AlLamy, A., 1996. Evaluating pore structure and morphology of hydrocarbon-conversion catalysts. Deactiv. Test. Hydrocarb. Process. Catal. 634, 42–60.
Peden, C.H.F., Goodman, D.W., 1987. Kinetics of cyclohexane dehydrogenation and hydrogenolysis over Ru(001) and Cu/Ru(001). J. Catal. 104, 347–358.
Riikonen, J., Salonen, J., Lehto, V.P., 2011. Utilising thermoporometry to obtain new insights into nanostructured materials. J. Therm. Anal. Calorim. 105, 811–821.
Rouquerol, F., Rouquerol, J., Sing, K., 1999. Adsorption by Powders and Porous Solids: Principles, Methodology and Applications. Academic Press, London.
Schreiber, A., Ketelsen, I., Findenegg, G.H., 2001. Melting and freezing of water in ordered mesoporous silica materials. Phys. Chem. Chem. Phys. 3, 1185–1195.
Shah, A., Fishwick, R.P., Wood, J., Leeke, G., Rigby, S.P., Greaves, M., 2010. A review of novel techniques for heavy oil and bitumen extraction and upgrading. Energy Environ. Sci. 3, 700–714.
Shiko, E., Edler, K.J., Lowe, J.P., Rigby, S.P., 2012. Probing the impact of advanced melting and advanced adsorption phenomena on the accuracy of pore size distributions from cryoporometry and adsorption using NMR relaxometry and diffusometry. J. Colloid Interface Sci. 385, 183–192.
Shiko, E., Edler, K.J., Lowe, J.P., Rigby, S.P., 2013. Probing hysteresis during sorption of cyclohexane within mesoporous silica using NMR cryoporometry and relaxometry. J. Colloid Interface Sci. 398, 168–175.